11th International Symposium on Magnetic Bearings
August 26-29, Nara, Japan

DEVELOPMENT OF A LORENTZ-FORCE-TYPE SLOTLESS SELF-BEARING MOTOR

Satoshi Ueno, Shin-ichi Uematsu and Takahisa Kato
Dept. of Mechanical Eng., Faculty of Science and Technology, Ritsumeikan Univ., Kusatsu, Shiga 525-85777 Japan
sueno@se.ritsumei.ac.jp

ABSTRACT

Magnetic bearings have advantages such as no friction loss, no abrasion, and lubrication-free operation. However they are not widely used due to their high cost and large size. In order to solve these problems, a self-bearing motor having a simple structure with distributed windings is proposed. The rotor consists of a permanent magnet and an iron yoke, which rotate in a body. The stator consists of a six-phase distributed winding and is installed between a permanent magnet and a back yoke of the rotor. A Lorentz force is generated by the stator current, and the rotation speed and radial position of the rotor are controlled by this force. In this study, the rotating torque and bearing force are analyzed theoretically, and a method for their control is discussed. A simple experiment confirms that the proposed self-bearing motor can be realized.

INTRODUCTION

In recent years, there has been an increasing demand for improving the durability of small motors and reducing the noise generated by them [1-4]. A magnetic bearing is useful in satisfying these demands. Various types of small motors that use an active magnetic bearing (AMB) or a self-bearing motor have been proposed. However, the AMB is not widely used since it is expensive and its dimensions are significantly larger than those of mechanical bearings. As a result, the development of a smaller and relatively low cost AMB is desired.

In order to satisfy this demand, a six-salient-pole-type AMB has been proposed [2]. The miniaturization and reduction in the cost of the AMB have been achieved by reducing the number of salient poles and coils in a conventional magnetic bearing. However, since the miniaturization and large bearing force are reconciled, the structure has become complicated. As a result, further miniaturization of the six-salient-pole-type AMB is difficult, and a simpler structure is required.

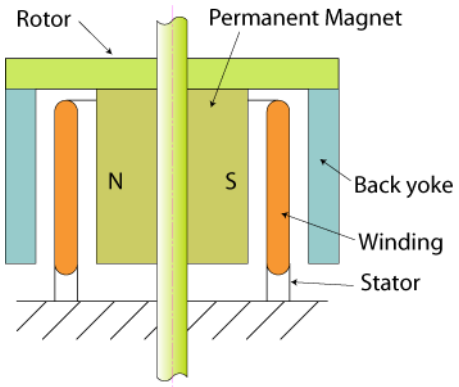

FIGURE 1: Schematic of Slotless SBM

In recent years, a miniaturized brushless DC motor has been developed. In particular, the miniaturization of a slotless stator-type motor has been remarkable, and it is commercially available as a motor with a diameter of 2mm. Since the magnetic bearing has a structure that is similar to that of the brushless motor, the structure of a miniaturized magnetic bearing can be modeled similar to that of a micro brushless DC motor. Then we propose a Lorentz-force-type slotless AMB [4]. A schematic drawing of the proposed AMB is shown in figure 1. A distributed winding without an iron core is installed in a stator, and a cylindrical permanent magnet fixed to a yoke is attached to a rotor. Subsequently, a bearing force is generated in accordance with a Lorentz force produced by the stator current and a magnetic field produced by the permanent magnet. Usually, the force that can be generated by an AMB by employing the Lorentz force is smaller than that generated by a typical magnetic bearing [5]. For this reason, it is necessary to supply large currents in order to negate the unstable force of the permanent magnet; however, this results in a decrease in the power consumption. In order to prevent the occurrence of this problem, the permanent magnet of the rotor is fixed to the yoke; as a result, the unstable force of

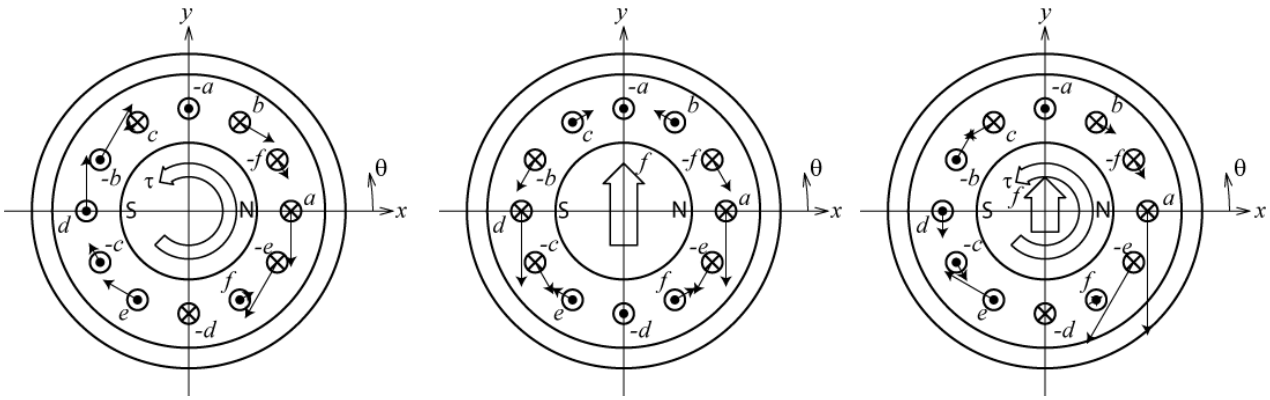

(a) Rotating Torque (b) Bearing Force (c) Rotating Torque and Bearing Force

FIGURE 2: Generation of Rotating Torque and Bearing Force

the permanent magnet becomes zero. The proposed magnetic bearing has a simple structure; therefore, its miniaturization and cost reduction can be achieved.

In this study, a self-bearing motor having a structure similar to that of a slotless AMB has been proposed. By combining an AC motor and a magnetic bearing, the AMB can be miniaturized further and its price can be reduced. The bearing force and rotation torque are analyzed theoretically, and a method for their control is derived. The result of the analysis is then confirmed using a simple experimental setup.

SLOTLESS SELF-BEARING MOTOR

The outline of the proposed self-bearing motor is shown in figure 1. The self-bearing motor carried out position control with two radial degrees of freedom and generates a motor torque. A rotor consists of a cylindrical two-pole permanent magnet and an iron yoke. The unstable attractive force of the permanent magnet becomes zero since an airgap between the permanent magnet and iron yoke does not change. The stator consists of a six-phase distributed winding without a core, and it is inserted between the permanent magnet and the yoke of the rotor.

The principle of generation of a torque and force is shown in figure 2. For simplicity, the figure illustrates the case in which the number of turns of the stator winding is one. If currents are supplied to the stator winding as shown in figure 2 (a), a Lorentz force is generated as denoted by the black arrows in the figures. Consequently, a motor torque is generated on the rotor as a reaction force. On the other hand, if currents are supplied as shown in figure 2 (b), a bearing force is generated as shown in the figure. By supplying the summation of the torque current and bearing current as shown in figure 2 (c), both the motor torque and bearing force are generated.

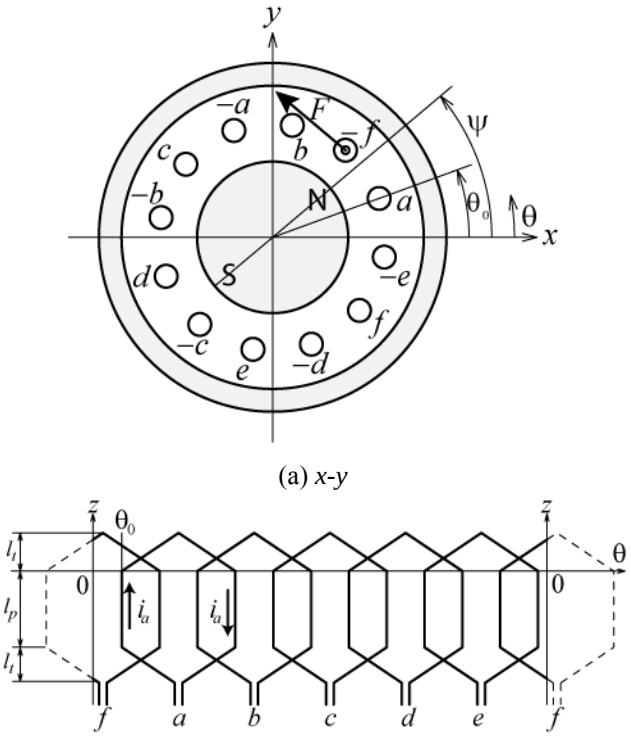

(a) *x*-*y*

(b) *z*-θ

FIGURE 3: Coordinate Axis

The motor torque and bearing force are controlled by changing the amplitude and the phase of stator current.

Radial Force and Rotating Torque

Figure 3 shows the coordinate axis used for the analysis of the rotating torque and bearing force. Figure 3 (a) shows the section perpendicular to the motor shaft, and figure 3 (b) shows the development along the

circumference of the stator winding. A magnetic flux that travels to the outside of the rotor is defined as positive.

The winding has a hexagonal shape as shown in figure 2. Hence, it can be divided two parts. One is the center of the winding, that is parallel to the axial direction. The other part comprises the top and bottom parts of the winding, and is slanted to turn the direction of the wire. The angular positions of the parallel part are expressed as

$$\begin{aligned}\theta^k_{+phase} &= \theta_0 + \frac{k-1}{3n}\pi + \frac{2m}{6}\pi \\ \theta^k_{-phase} &= \theta_0 + \frac{k-1}{3n}\pi + \frac{2m+3}{6}\pi\end{aligned} \tag{1}$$

where m is the coefficient corresponding to each phase, a-phase→0, and f-phase→5, n is the total number of turns, k is the turn number, and θ_0 is the angular position of the +a-phase winding.

In order to simplify the analysis, it is assumed that the magnetic field generated by the current is weaker than that generated by the permanent magnet of the rotor, and a sinusoidal waveform distribution of the magnetic flux density is obtained. Then, the magnetic flux density distribution in the airgap is

$$B_g(\theta) = B\cos(\theta - \psi) \tag{2}$$

where B is the amplitude of the magnetic flux density, and ψ is the angular position of the rotor. The stator currents are the summation of the bearing current and motoring current. Hence, the currents are expressed as follows.

$$\begin{aligned}i_{a,d} &= i_d\cos(\psi) + i_q\sin(\psi) \pm A_m\cos(\phi_m) \\ i_{b,e} &= i_d\cos(\psi - \frac{2\pi}{3}) + i_q\sin(\psi - \frac{2\pi}{3}) \mp A_m\cos(\phi_m - \frac{4\pi}{3}) \\ i_{c,f} &= i_d\cos(\psi - \frac{4\pi}{3}) + i_q\sin(\psi - \frac{4\pi}{3}) \pm A_m\cos(\phi_m - \frac{2\pi}{3})\end{aligned} \tag{3}$$

where i_d is the direct axis current, i_q is the quadric axis current, A_m is the amplitude of the motor current, and ϕ_m is its phase.

First, the case of n = 1 is considered. The Lorentz force is calculated by Fleming's law as

$$f_{\pm phase} = \mp B_g(\theta_{\pm phase}) i_{phase} l_p \tag{4}$$

where l_p is the length of the parallel part. The torque produced by the Lorentz force becomes

$$\tau_{\pm phase} = r f_{\pm phase} \tag{5}$$

where r is the radius of the winding. The radial force becomes

$$\begin{aligned}f_{x\pm phase} &= -f_{\pm phase}\sin(\theta_{\pm phase}) \\ f_{y\pm phase} &= f_{\pm phase}\cos(\theta_{\pm phase})\end{aligned} \tag{6}$$

The total torque and force are the summation of (5) and (6), respectively. Then we have

$$\begin{aligned}\tau &= -3rl_pBA_m\sin(\phi_m - \psi + \theta_0 + \pi/4) \\ f_{x\pm phase} &= 3l_pB\{i_d\sin(2\theta_0) + i_q\cos(2\theta_0)\} \\ f_{y\pm phase} &= -3l_pB\{i_d\cos(2\theta_0) + i_q\sin(2\theta_0)\}\end{aligned} \tag{7}$$

The angular position of the turn part can be expressed as follows.

$$\begin{aligned}\theta_{t+phase}(z) &= \frac{\pi}{4l_t}z + \frac{2m}{6} + \theta_0 \\ \theta_{t-phase}(z) &= \frac{2m+3}{6} - \frac{\pi}{4l_t}z + \theta_0\end{aligned} \tag{8}$$

where l_t is the length of the turn part. The Lorentz force of a small distance in this part is calculated as

$$\Delta f_{t\pm phase} = \mp B_g(\theta_{t\pm phase}(z))\cdot i_{phase}\cdot\frac{\Delta z}{\sin\alpha} \tag{9}$$

where α is a wire angle with its horizontal axis passing through the turn part, and it is expressed as

$$\alpha = \tan^{-1}\frac{\theta_{+phase} - \theta_{-phase}}{2l_p}r = \tan^{-1}\frac{\pi r}{4l_p} \tag{10}$$

The Lorentz force in the turn part consists of two components force in the axial direction, Δf_{tz}, and force in the radial direction, Δf_{tt}. Each force is expressed as follows.

$$\begin{aligned}\Delta f_{tz} &= \Delta f_t\cos\alpha \\ \Delta f_{tt} &= \Delta f_t\sin\alpha\end{aligned} \tag{11}$$

The force in the radial direction becomes

$$\Delta f_{tt\pm phase} = \mp B_g(\theta_{t\pm phase}(z)) i_{phase}\Delta z \tag{12}$$

and the torque at the turn part is calculated as follows.

$$\tau_{\pm phase} = \int_0^{l_t} r f_{tt\pm phase} \tag{13}$$

Then the total torque becomes

$$\tau = -\frac{4rl_tBA_m}{\pi}(6 - 3\sqrt{2})\sin(\phi_m - \psi + \theta_0 + \pi/4) \tag{14}$$

The radial force of each phase is calculated as

$$\begin{aligned}f_{x\pm phase} &= -\int_0^{l_t} f_{tt\pm phase}\cdot\sin(\theta_{t\pm phase}(z)) \\ f_{y\pm phase} &= -\int_0^{l_t} f_{tt\pm phase}\cdot\cos(\theta_{t\pm phase}(z))\end{aligned} \tag{15}$$

The total radial force is the summation of the forces of all phases, then,

$$\begin{aligned}f_x &= \frac{6l_tB}{\pi}\{i_d\sin(2\theta_0) - i_q\cos(2\theta_0)\} \\ f_y &= -\frac{6l_tB}{\pi}\{i_d\cos(2\theta_0) + i_q\sin(2\theta_0)\}\end{aligned} \tag{16}$$

Since the turn part comprises two parts, the total torque and radial force become

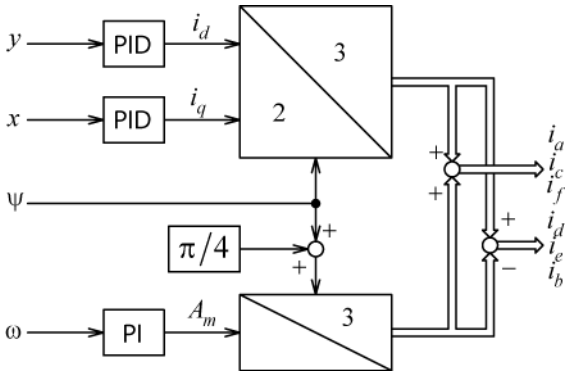

FIGURE 4: Closed-loop Torque Controller

$$\begin{aligned} \tau &= k_m A_m \sin(\phi_m - \psi + \theta_0 + \pi/4) \\ f_x &= -k_b \left\{ i_d \sin(2\theta_0) - i_q \cos(2\theta_0) \right\} \\ f_y &= k_b \left\{ i_d \cos(2\theta_0) + i_q \sin(2\theta_0) \right\} \end{aligned} \tag{17}$$

where

$$\begin{aligned} k_m &= -\left(3l_p + \frac{8(6-3\sqrt{2})}{\pi} l_t \right) rB \\ k_b &= -\left(3l_p + \frac{12}{\pi} l_t \right) B \end{aligned} \tag{18}$$

For n = 3, the interval between the phases of the wires is π/9. Therefore, the rotating torque can be expressed the summation of (16), where θ_0=−π/9, 0, and π/9. Then, we have

$$\tau = k_m A_m \sin(\phi_m - \psi + \theta_0 + \frac{\pi}{4}) \left\{ 1 + 2\cos(\frac{2\pi}{9}) \right\} \tag{19}$$

Similarly, the following equations are obtained.

$$\begin{aligned} \tau &= k_n k_m A_m \sin(\phi_m - \psi + \theta_0 + \pi/4) \\ f_x &= -k_n k_b \left\{ i_d \sin(2\theta_0) - i_q \cos(2\theta_0) \right\} \\ f_y &= k_n k_b \left\{ i_d \cos(2\theta_0) + i_q \sin(2\theta_0) \right\} \end{aligned} \tag{20}$$

where

$$\begin{aligned} k_n = 1 &+ 2\cos\left(\frac{2\pi}{3n}\right) + 2\cos\left(\frac{4\pi}{3n}\right) + \\ &\cdots + 2\cos\left(\frac{(n-1)\pi}{3n}\right) \end{aligned} \tag{21}$$

Closed-loop Torque Control

If the angular position of the rotor can be obtained, the stator current can be calculated by (4). Then, assuming θ_0=0 and $\phi_m - \psi + \theta_0 + \pi/4 = \pi/2$, the rotating torque and bearing force become

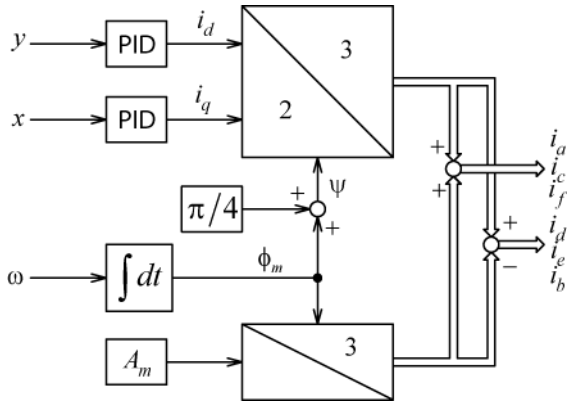

FIGURE 5: Open-loop Torque Controller

$$\begin{aligned} \tau &= k_n k_m A_m \\ f_x &= k_n k_b i_q \\ f_y &= k_n k_b i_d \end{aligned} \tag{22}$$

Hence, the rotating torque can be controlled by A_m, and the bearing force can be controlled by i_d and i_q.

The block diagram of a closed-loop torque controller is shown figure 4. The radial position controller is a standard PID controller, while the rotating speed controller is a PI controller.

Open-loop Torque Control

If the angular position of the rotor cannot be obtained, the rotating torque can be passively controlled by a current with constant amplitude and frequency. Let $\phi_m = \omega t$ and the phase difference between ϕ_m and ψ denoted by $\Delta\phi_m = \phi_m - \psi + \pi/4$ then, we have

$$\tau = k_n k_m A_m \sin(\Delta\phi_m) \tag{23}$$

Hence, the torque is passively controlled by $\Delta\phi_m$. If a load torque is small, that is $\Delta\phi_m \approx 0$, ψ can be approximate to $\pi/4 + \phi_m$. Therefore the stator current can be calculated by substituting $\psi = \pi/4 + \phi_m$ in equation (3).

The block diagram of an open-loop torque controller is shown in figure 5. An angular position detector is not required; therefore, the control system becomes simpler.

EXPERIMENTAL RESULTS

Experimental Setup

In order to confirm the above mentioned results, a simple experimental setup was designed and tested. The experimental setup is shown in figure 6. For simplicity,

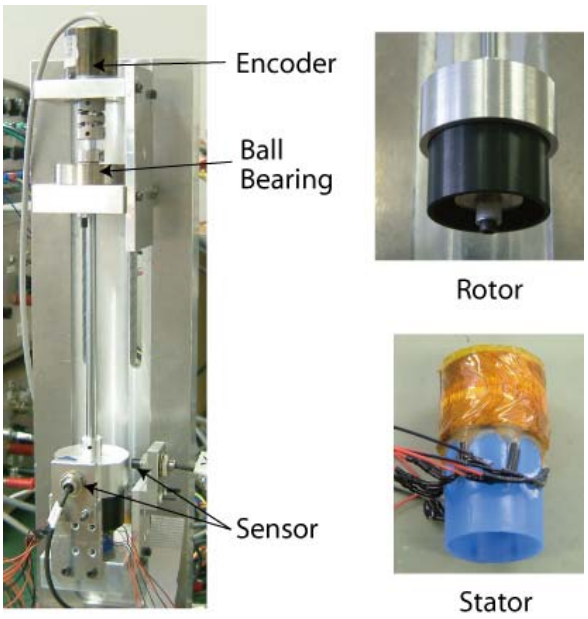

FIGURE 6: Experimental Setup

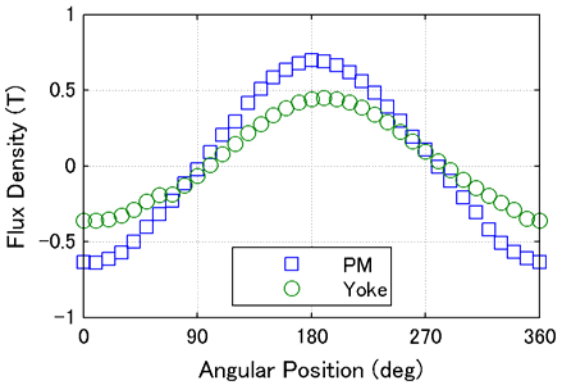

FIGURE 7: Flux Density Distribution

the rotor top was supported using a ball bearing; therefore, the rotor had three degrees of freedom x, y, and around z. The self-bearing motor was attached to the lower part of the rotor, and a rotary encoder was attached to the upper part for measuring the angular position of the rotor.

The rotor consisted of a shaft, permanent magnet, back yoke, and one part to fix them together. A two-pole cylindrical neodymium magnet was used. The outer diameter, inner diameter and length of the permanent magnet were 22 mm, 8 mm, and 22 mm, respectively. The back yoke was composed of S45C. Its outer and inner diameters are 38 mm and 34 mm, respectively. The distribution of the magnetic flux density between the permanent magnet and the back yoke is shown in figure 7.

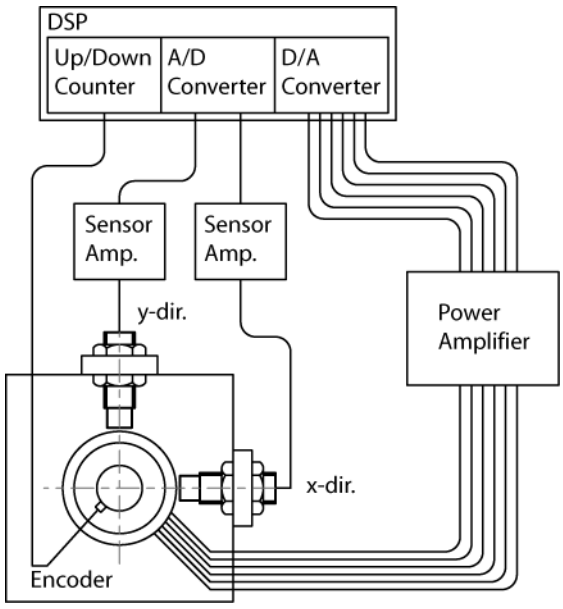

FIGURE 8: Control System

The curve drawn using the squares denotes the result of the flux density measured on the surface of the permanent magnet, and the curve drawn using the circles denotes the result of the flux density measured on the inner surface of the yoke. From these results, it is confirmed that the magnetic flux density distribution is sinusoidal, and its mean amplitude is approximately 0.6T.

The stator consists of the winding and a plastic collar for fixing it. The copper wire has diameter of 0.26mm and the number of turns is 55.

The control system is shown in figure 8. A digital signal processor (DSP) has been used for control. The DSP receives signals from two displacement sensors through A/D converters and the angular position of the rotor through an up/down counter. Then the DSP calculates the stator current. The stator currents are then output to a power amplifier through a D/A converter. A current-output-type amplifier is used as the power amplifier.

Motor Torque and Bearing Force

First, the results of measuring the motor torque are shown. While carrying out the position control, a constant torque current was supplied. The rotation of the rotor was stopped by a force applied using a force gauge connected to the shaft. Then, the rotating torque was calculated from the value of the force gauge. The result is shown in figure 9. From this result, it was confirmed that the torque was linear to the torque current. However, the measured

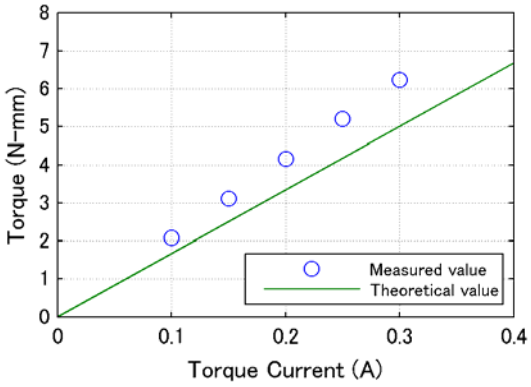

FIGURE 9: Rotating Torque

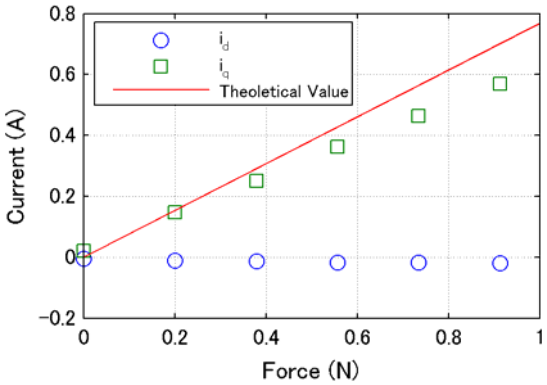

FIGURE 10: Bearing Force

values were larger than the theoretical values. One of the reasons for this was that the stator winding was not ideal.

The measurement results of the bearing force are shown in figure 10. While carrying out the position control of the rotor, a constant disturbance force was applied in the x direction, and the current was measured when the displacement became zero. The circles and square denote the i_d and i_q values, respectively. This result shows that the force is proportional to the current.

Impulse Responses

The impulse responses at 0 rev/min were measured for confirming the position control. The results are shown in figure 11. Figures 11 (a) and (b) show the results of the impulse responses obtained using the closed-loop torque controller, open-loop torque controller, respectively. Both these impulse responses settled in 0.2 s, which confirmed that stable control was carried out.

Rotation Test

Figure 12 shows a trajectory of the rotor motion in the x-y plane at 2,000 rev/min and 5,000 rev/min, obtained using the closed-loop torque controller. In both cases, the

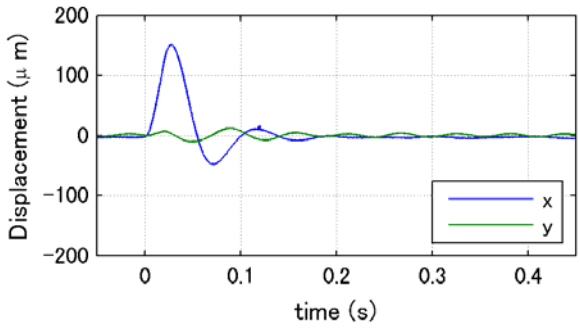

(a) Closed-loop Torque Controller

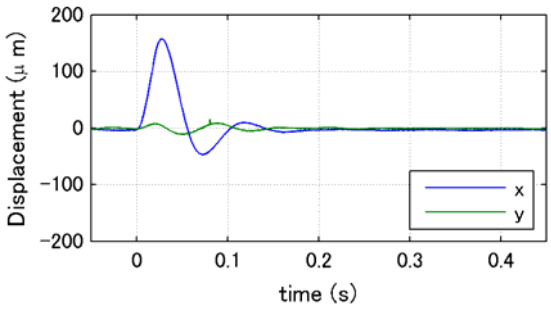

(b) Open-loop Torque Controller

FIGURE 11: Impulse Responses (0 rev/min)

amplitude of vibration was approximately 25 mm, and the rotor could rotate stably. Figure 13 shows the corresponding results obtained using the open-loop torque controller. In this case, the orbit was unstable compared to that obtained using the closed-loop torque controller. In particular, the orbit obtained at 5,000 rev/min was more unstable than that obtained at 2,000 rev/min. One of the possible reasons for this is that $\Delta\phi_m$ changes by a perturbation of the rotation torque. The change of $\Delta\phi_m$ causes an error of the bearing force, and it influences the radial position control. From these results, it is obvious that the closed-loop torque controller is suitable for achieving high-speed rotation. Hence, if the use of an encoder is not possible, a sensorless vector control method should be employed.

Finally, the acceleration test results are shown in figure 14. This test was performed using the closed-loop torque controller. The rotation speed was changed from 0 to 5,000 rev/min, and the motor current A_m, rotation speed, and displacement were measured. The torque current was limited to 0.4 A. The rotation speed became 5,000 rev/min after 2 s. Although the displacement deviated slightly from zero, it was confirmed that the rotor could be supported stably during the acceleration.

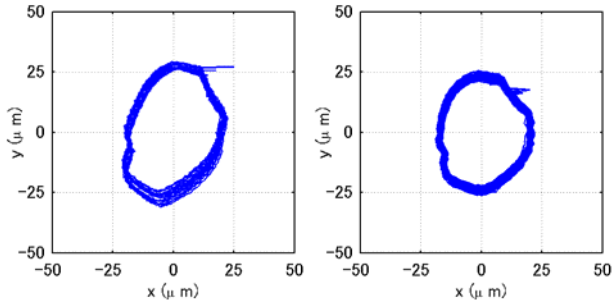

(a) 2,000 rev/min (b) 5,000rev/min

FIGURE 12: Orbit Obtained Using Closed-loop Torque Controller

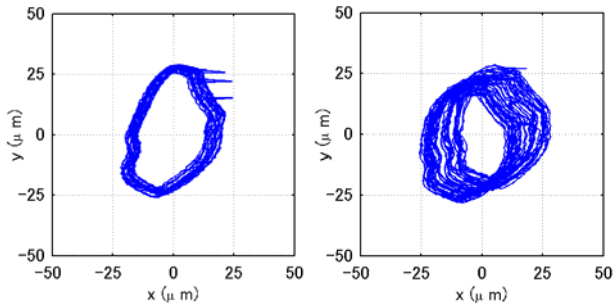

(a) 2,000 rev/min (b) 5,000rev/min

FIGURE 13: Orbit Obtained Using Open-loop Torque Controller

CONCLUSIONS

In this study, a novel self-bearing motor is proposed using a slotless distribution winding. The proposed self-bearing motor is capable of being miniaturize because it has a simple structure. The motor torque and bearing force are derived analytically, and a method for the control of the rotation speed and position is discussed. Experimental results show that the proposed self-bearing motor can be realized and it has high potential for high-speed rotation.

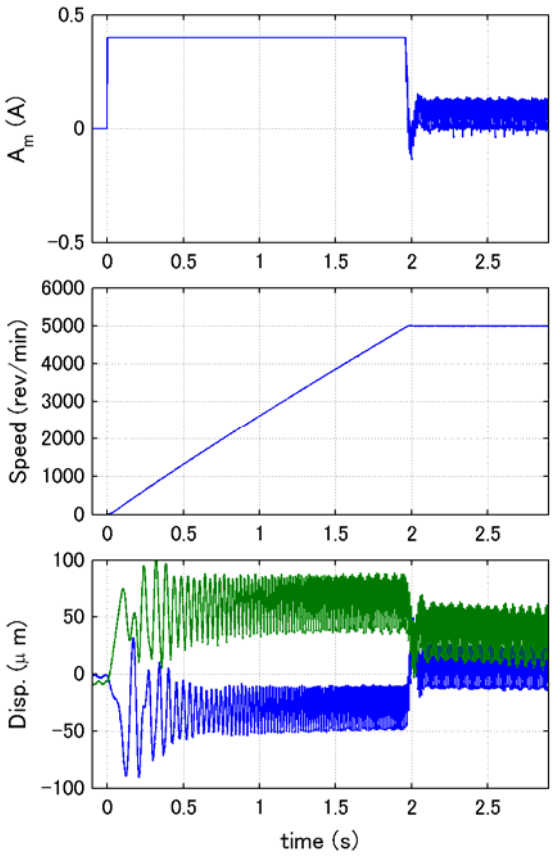

FIGURE 14: Acceleration Test

REFERENCES

1. Y. Okada et al., JSME Publication on New Technology Series, No. 1, Magnetic Bearings—Fundamental Design and Applications, Yokendo Ltd. Tokyo, 1995, in Japanese (translated into Korean).
2. S. Ueno et al., “Development of the Miniature AMB with 6 Concentrated Wound Poles”, ISMB-9, Lexington, KY, USA, 2004
3. L. Li et al., “A Simple and Miniaturized Magnetic Bearing for Cost-Sensitive Applications”, Proc of 8th Int. Symp. on Magnetic Bearings, Mito, August 26–28, 2002, pp. 561–565.
4. S. Ueno et al., “Development of a Lorentz-force-type Slotless Active Magnetic Bearing”, ISMB-10, Martigny, Switzerland, 2006
5. T. Tokumoto et al., “Comparison between Slot and Slotless Constructions of Lorenz Type Self-bearing Motor”, Trans. of JSME, Vol. 68, No. 674 C, pp. 2992–2998, 2002, in Japanese